Cell Reports
Physical Science

CellPress
OPEN ACCESS

Article

Advancing ionomer design to boost interfacial and thin-film proton conductivity via styrene-calix[4]arene-based ionomers

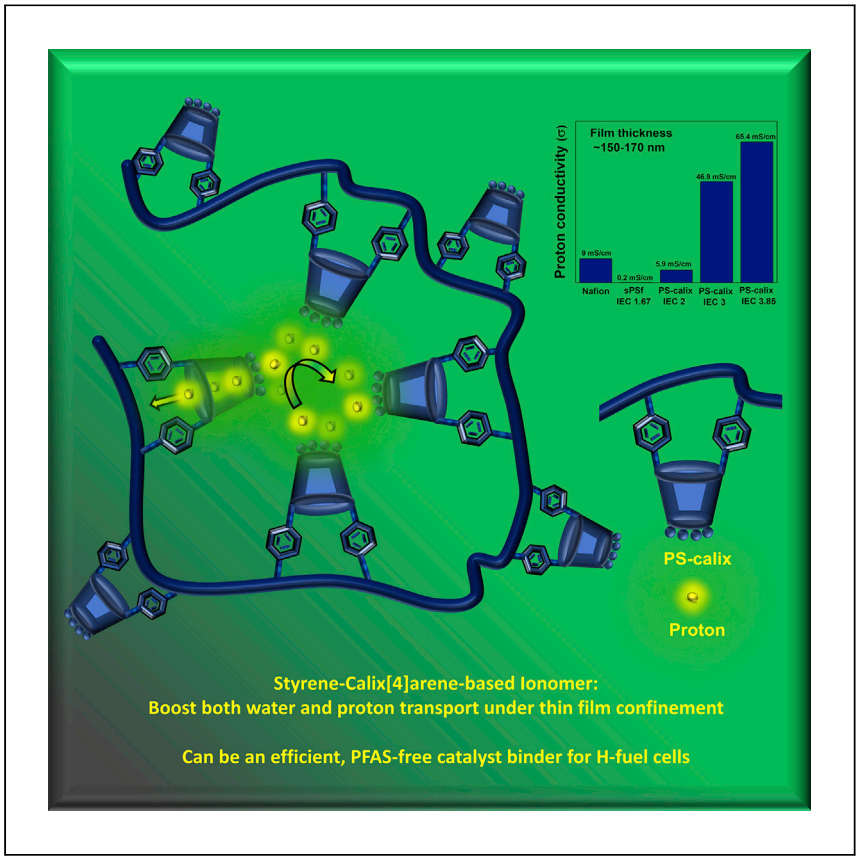

Chatterjee et al. incorporate sub-nanometer-sized macrocyclic cavities within the chemical structure of ionomers. This class of ionomer exceeds the water and proton transport performances of the state-of-the-art ionomer Nafion in thin materials, mimicking catalyst-binder layers of fuel cell electrodes.

Shyambo Chatterjee, Oghenetega Allen Obewhere, Ehsan Zamani, ..., Martha D. Morton, Anandakumar Sarella, Shudipto Konika Dishari

sdishari2@unl.edu

Highlights

A class of ionomer (PS-calix) leveraging sub-nanometer-sized cavities of calix[4]arene

PS-calix exhibits proton conductivity ~13 times higher than Nafion in thin films

Fast proton conduction is facilitated by faster-than-bulk water transport

Alleviates ion and gas transport limitations, desired for binders for fuel cells

Chatterjee et al., Cell Reports Physical Science 4, 101282
February 15, 2023
https://doi.org/10.1016/j.xcrp.2023.101282

Cell Reports
Physical Science

CellPress
OPEN ACCESS

Article

Advancing ionomer design to boost interfacial and thin-film proton conductivity via styrene-calix[4]arene-based ionomers

Shyambo Chatterjee,[1,4] Oghenetega Allen Obewhere,[1,4] Ehsan Zamani,[1] Rajesh Keloth,[1] Seefat Farzin,[1] Martha D. Morton,[2] Anandakumar Sarella,[3] and Shudipto Konika Dishari[1,5,*]

SUMMARY

Sub-micrometer-thick ion-conducting polymer (ionomer) layers often suffer from poor ionic conductivity at the substrate/catalyst interface. The weak proton conductivity makes the electrochemical reaction at the cathode of proton-exchange-membrane fuel cells sluggish. To address this, here we report on a class of polystyrene-based ionomers having sub-nanometer-sized, sulfonated macrocyclic calix[4]arene-based pendants (PS-calix). In films with thickness comparable to that of ionomer-based binder layers, the conductivity of PS-calix film (~41 mS/cm) is ~13 times higher than that of the current state-of-the-art ionomer, Nafion. We observe a similar improvement in proton conductivity when PS-calix interfaces with Pt nanoparticles, demonstrating the potential of PS-calix in catalyst ink. Leveraging a favorable interfacial chemical composition, PS-calix enhances proton conduction at the film-substrate interface, a shortcoming of Nafion. Moreover, the water in PS-calix films diffuses faster than bulk water and the water confined in Nafion films, suggesting an important role played by sub-nanometer-sized calix[4]arene cavities in creating unique water/ion transport pathways.

INTRODUCTION

The proton-exchange-membrane fuel cell (PEMFC) is a unique, eco-friendly electrochemical device that can electrify and power automobiles, space shuttles, submarines, and many portable/stationary appliances. To generate electricity, PEMFCs utilize H_2 as a fuel, which can offer specific energy three times higher than gasoline, the primary fuel of internal combustion engines (ICEs). To excel in PEMFC technology and compete with ICE-based vehicles, we still need to strike the cost-performance-durability targets set by the US Department of Energy (DOE).[1,2] A major requirement is to lower the loading of expensive platinum group metal (PGM) catalysts (from 0.25 to 0.0625 g PGM/kW, or from 0.4–0.8 to 0.05 mg PGM/cm^2),[3] with a working current density of 3–4 A/cm^2 at 0.7–0.8 V.[4] As catalyst loading is reduced, to maintain satisfactory oxygen reduction reaction (ORR) activity, we must overcome ion (proton) and gas (O_2) transport limitations at the interface of catalyst and ion-conducting polymers (ionomers). In PEMFCs, ionomers are not only used as membrane separators transporting protons from anode to cathode but are also used as catalyst binders and ion transporters to the catalyst active sites on electrodes. The thicknesses of the ionomer-based membrane and the binder layer are different: the membranes are typically several tens of micrometers thick, while the ionomer binder layers are several tens of nanometers thick. Designing ionomers to make

[1]Department of Chemical and Biomolecular Engineering, University of Nebraska-Lincoln, Lincoln, NE 68588, USA

[2]Department of Chemistry and Nebraska Center for Integrated Biomolecular Communication, University of Nebraska-Lincoln, Lincoln, NE 68588-0304, USA

[3]Nebraska Center for Materials and Nanoscience, Voelte-Keegan Nanoscience Research Center, University of Nebraska-Lincoln, Lincoln, NE 68588-0298, USA

[4]These authors contributed equally

[5]Lead contact

*Correspondence: sdishari2@unl.edu

https://doi.org/10.1016/j.xcrp.2023.101282

efficient membrane separators has been extensively pursued.[5–11] To improve the performance of the ionomer-catalyst layer, on the other hand, the emphasis has mostly been on designing new catalysts[12–15] and catalyst layer nanostructures.[16–23] However, designing ionomers to fulfill the specific requirements of a catalyst binder layer is still very limited.[24–28] To date, the ionomers designed for membrane separators (like Nafion) have been used as binders as well.

It is just in the past two decades that researchers have revealed and realized that ionomer behavior, when confined in sub-micrometer-thick films (as in ionomer binder layer), can be drastically different from that of its bulk membrane counterpart.[24,29–34] For example, the proton conductivity of the current state-of-the-art ionomer Nafion in a bulk free-standing membrane (~25 μm thick) is about an order of magnitude higher than that of Nafion in a 25-nm-thick, spin-coated film in the hydrated state.[24,30,31] To identify the reasons behind the ion transport limitations, efforts are being made to fundamentally understand the thin-film properties of proton-conducting ionomers. The understanding in this area is gradually evolving based on the insights obtained primarily from Nafion[25,34–45] and a few hydrocarbon-based ionomers[24,25,46,47] in thin films. The ion conduction in sub-micrometer-thick ionomer films or at the ionomer-substrate interface is governed by a complicated matrix of interdependent factors,[31–33,48] such as dimensional constraints (thin-film confinement),[24,25,30,34,35,37,40,41,47] constraints due to ionomer-water interfacial interactions,[29,38,40,41,] hydrophilic-hydrophobic phase segregation,[34,37] ionic domain size,[35,37] spacing,[34,37] distribution,[30] connectivity,[37,40] water uptake,[24,25,34,37,40,41,47] swelling,[34,47] and more. Especially, poor phase separation and resulting small, scattered, and disconnected ionic domains/ion channels[34,37,40] have been identified as some of the major issues negatively affecting thin-film ionic conductivity. For example, Modestino et al.[34] and Farzin et al.[37] showed a high degree of phase mixing in transmission electron microscopy (TEM) images as the film thickness of fluorocarbon-based ionomers decreased. The phase mixing corroborated with the gradually diminishing ionic domain peaks in grazing-incidence small-angle X-ray scattering (GISAXS) studies.[18,34,38,39] Interestingly, in several cases, the water uptake of ionomer thin films was reasonably high (even higher than that of the bulk membranes),[37,40] but still the proton conductivity was lower than that of bulk membranes. The average size of ionic domains in these thin Nafion films (~1–2 nm)[37] was smaller than that in bulk Nafion membranes (~4 nm).[49] It appeared that ~1- to 2-nm-sized ionic domains with poor interconnectivity caused very weak proton conductivity, no matter how high the water sorption by the ionomer films was.[35,37,40] This suggested that having control over the size and connectivity of ionic domains is critical to attain extended proton hopping pathways and improve thin-film ionic conductivity. In our recent work, we looked beyond the average ion conduction properties and found that the ion conduction environment can be very different at different depths within an ionomer film. In Nafion thin films, proton conduction was very weak next to the substrate and gradually went higher as the air interface was approached.[30] This was attributed to the interactions happening at the substrate interface among ionomer, water, and substrate functionalities. Such interfacial interactions can be detrimental to water-polymer mobility[25,40,41,47,50] and, therefore, proton conduction.[25,30,40] Not only that, strong adsorption of ionomer chains on catalyst particles can cover the catalyst active sites to an extent that leads to O_2 transport resistance.[51,52] The lower electrochemically active surface area of catalysts has caused poor proton and gas transport for Nafion and several aromatic ionomers.[33,35,46,53] This suggested that any ionomer capable of addressing these issues could be beneficial to the design of more efficient ionomer-catalyst layers on electrodes.

To alleviate the ion transport limitation, we need ionomers that can strategically design ion-conducting channels. Porous organic/inorganic materials, such as polymers with intrinsic microporosity (PIMs),[54] metal-organic frameworks (MOFs),[55] covalent organic frameworks (COFs),[56,57] and electrospun hollow nanofibers,[58] have been designed that can create channels for water, gas, and ion transport. A major fraction of these porous systems relies on the interconnectivity of channels, and the hollow cavities/channels in these systems have diameters above 1 nm to facilitate transport. Materials having sub-nanometer-sized hollow constrictions are creating a buzz by transporting water and ions much faster. This class of materials is mostly inspired by natural water- and ion-transporting channels like gramicidin A.[59] Gramicidin A is a biological ion channel with a diameter of ~4 Å. While the understanding of transport through such narrow constrictions is still an ongoing process, and there are different trains of thought based on experimental and computational efforts,[60–68] a plausible mechanism put forward suggests that sub-nanometer sized channels allow the formation of single strands of H-bonded water molecules, known as 1D water wires.[66,67] In such a narrow channel with a hydrophobic interior, water can experience frictionless or slip flow[69] and diffuse much faster than bulk water. Also, while the H-bonded water network in bulk water is more branched and random, the H-bonded path in 1D water wires is more controlled, with preferentially aligned water dipoles facilitating faster proton hopping.[66–68] Inspired by natural water and ion channels, a range of synthetic materials have been developed that have been majorly demonstrated for host-guest interaction, sensing, water/solvent/gas/chemical purification, pharmaceutical, and blue energy harvesting applications.[64,70–78] Some of the materials having sub-nanometer constrictions include imidazole quartets[79]; triazole channels[80]; hexa(*m*-phenyleneethynylene) channels[81]; aquafoldamers[82]; peptide-,[83] hydrazide-,[84] or ester-appended monomeric/dimeric pillar[n]arenes[85]; MOFs[86]; graphene[87,88]; cyclic peptide nanotubes[89]; carbon nanotubes (CNTs)[68,90,91]; and cavity-forming polymers.[24] One of the notable observations was by Noy and colleagues,[90] showing how the water and ion transport performance can be influenced by >1- and <1-nm-sized CNTs. The proton transport rate was similar to that of bulk water when the diameter of the CNTs was ~1.5 nm, but when the diameter went below 1 nm (~0.8 nm), the protons moved faster than those in bulk water. They attributed this faster-than-bulk water transport to the 1D water wire effect, which was also validated by simulations of CNTs.[68,92,93] Not only in CNTs,[90] but also in some other sub-nanometer-sized systems,[79–81,85,94–96] water and ions both got transported. In such studies, factors like the driving force to move water from the surrounding channels (more bulk-like) into the sub-nanometer sized channels,[60,63,94,97] functionality[61,62,81,85,96,98,99] and hydrophobicity[63,90] of the channel interior as well as the terminals, water dipole orientation across the water wire,[65–67,79,81] and reorientation relaxation[59,66,90] have been considered critical for proton transport through the channels. Typical ionomers, like Nafion, do not have sub-nanometer constrictions and thus cannot avail themselves of the 1D water wire and fast proton conduction,[90] like gramicidin A or CNTs.

In our recent work, we have been able to successfully translate the fast proton-conduction capability to a set of oligomeric model ionomers by incorporating sub-nanometer-sized hollow macrocyclic calix[4]arene cavities within the chemical structure of the ionomers.[24] The motivation behind this ionomer design was the intriguing differences in water and ion transport capabilities of ~1- to 2- and <1-nm-sized ionic domains/ion channels. The diameter of calix[4]arene is ~3 Å[100] (can vary up to +2 Å depending on the substituting groups[101]), and we saw an unprecedentedly high proton conductivity in sub-micrometer-thick films of these calix[4]arene-containing ionomers (calix-2). In addition, we showed experimental and computational

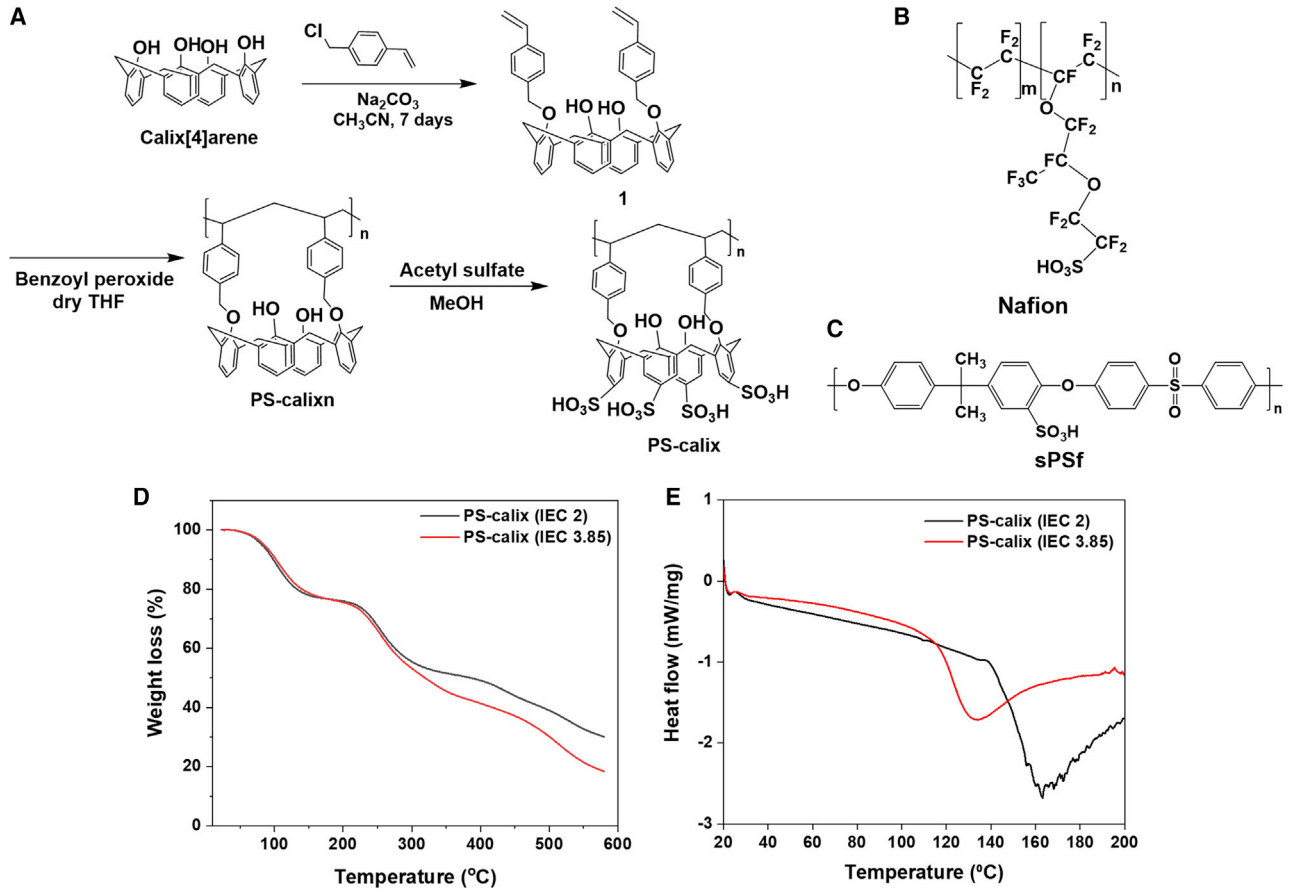

Figure 1. Synthetic procedure and thermal properties of PS-calix

(A) Synthetic scheme for the ionomer PS-calix.

(B and C) Chemical structure of Nafion (B) and sulfonated polysulfone (sPSf) (C).

(D) Thermogravimetric analysis (TGA) thermograms and (E) differential scanning calorimetry (DSC) of PS-calix with IECs 2 and 3.85.

evidence supporting the role of macrocycles in improving ionic conduction and selective ion permeation.[24] The results clearly indicated the high potential of calix[4]arene-based ionomers in addressing ion transport limitation and permselectivity critical for energy conversion and storage technologies.

Herein, we report a new class of macrocycle-based, polymeric ionomer (PS-calix), which consists of a polystyrene-based backbone and sulfonated calix[4]arene-based pendants. While there have been a few reports on polystyrene-based ionomers,[102–105] the incorporation of macrocycles within the chemical structure of polystyrene-based ionomers is very new. We examined the thin-film proton conduction and water self-diffusion behavior of PS-calix (Figure 1A) in comparison with traditional ionomers (Nafion and sulfonated polysulfone [sPSf]; Figures 1B and 1C) using electrochemical impedance spectroscopy (EIS) and diffusion-ordered nuclear magnetic resonance (DOSY NMR) spectroscopy, respectively. We also showed how PS-calix can manipulate and significantly improve the overall as well as depth-specific ion conduction behavior of ionomer thin films (confocal laser scanning microscopy [CLSM]). The stronger ion conduction behavior near substrate interfaces was rationalized based on the trends observed in viscoelastic properties (contact resonance atomic force microscopy [CR-AFM]) and depth-specific elemental analysis (scanning

electron microscopy with energy-dispersive X-ray spectroscopy [SEM/EDX]). Last but not least, we looked into the performance of PS-calix in pseudo-catalyst systems showing the great potential of PS-calix in addressing both gas and ion transport limitations. The added advantage of PS-calix could be its perfluoroalkyl substance (PFAS)-free nature, making it an eco-friendly and efficient substitute for the perfluorinated ionomer Nafion.[106]

RESULTS AND DISCUSSION

Chemical synthesis of ionomers

The synthesis of PS-calix ionomers (Figure 1A) started with the synthesis of monomeric divinylbenzylcalix[4]-arene derivative (1). Monomer 1 was synthesized with 80% yield by reacting calix[4]arene with 4-vinylbenzyl chloride in the presence of anhydrous sodium carbonate (Na_2CO_3) as a base. The ^{1}H NMR peak at 5.06 ppm (Ar [calix[4]arene] OC**H**$_2$Ar [styrene]) confirmed the attachment of vinyl benzene to calix[4]arene, while the peaks at 5.28 (–CH=CH**H**), 5.81 (–CH=C**H**H), and 6.66 (–C**H**=CH$_2$) ppm confirmed the presence of a terminal vinyl group (C=C double bond) in monomer 1 (Figure S1). Subsequent polymerization of monomer 1 was carried out in dry tetrahydrofuran (THF) using benzoyl peroxide as an initiator to yield PS-calixn, the neutral precursor of PS-calix ionomers (Figure 1A). The vinyl proton peaks between 5 and 6.6 ppm disappeared, and aliphatic proton peaks due to the bridging of vinyl benzene units (1.12–1.27 ppm) appeared in ^{1}H NMR (Figure S2), indicating successful polymerization of monomer 1 to PS-calixn. Both monomer 1 and PS-calixn retained the cone conformation of macrocyclic calix[4]arene as confirmed by the signature peaks in ^{1}H NMR (~3.35 and ~4.35 ppm, doublets). Subsequent reaction of PS-calixn with freshly prepared acetyl sulfate gave the sulfonated ionomers (PS-calix). The ratio of PS-calixn to acetyl sulfate was varied to obtain PS-calix with ion-exchange capacities (IECs) of 2 (1:1), 3 (1:2), and 3.85 (1:2.5). To confirm the success of sulfonation, the Fourier transform infrared (FTIR) spectra of non-sulfonated (PS-calixn) and sulfonated polymers (PS-calix, IEC 2, 3.85) were compared (Figure S3). The asymmetric and symmetric –S=O stretching (1,151, 1,090 cm^{-1}) as well as –S–O stretching (903 cm^{-1}) peaks were clearly seen in sulfonated ionomer (PS-calix). The C–S stretching peak at 683 cm^{-1} also appeared upon sulfonation. In addition, the –OH stretching peak (3,363 cm^{-1}) became slightly more intense upon sulfonation because of the additional –OH from the –SO_3H groups in PS-calix. The elemental analysis (wt %) showed 12.78% S in PS-calix (IEC 3.85), which was close to the theoretical value (12.74% S). The experimental (4.23) and theoretical (4.48) C:S ratios for this sample were also similar (Table S1). PS-calix ionomers with all IECs (2–3.85) were soluble in dimethylacetamide (DMAc), and not soluble in water, which is critical for the practical applications of these ionomers in energy conversion and storage devices. Also, when spin-coated into sub-micrometer-thick films on appropriate substrates, PS-calix formed smooth films.

Thermal properties

In PS-calix samples, three major thermal degradations were observed (Figure 1D): (1) gradual dehydration up to 150°C; (2) the decomposition of –SO_3H groups,[107] which was often ascribed to 200°C–300°C; and (3) aromatic backbone degradation, which could be attributed to 350°C–550°C.[108] The glass transition temperature (T_g) values (Figure 1E) of dry PS-calix samples ranged between 130°C and 176°C, which were higher than that for pure polystyrene (T_g ~100°C).[109,110] This could be attributed to the bulky side chain (made of sulfonated calix[4]arene) in PS-calix. Please note that this T_g was measured for the powdery polymer in a dry state. Like any polymer, the T_g of PS-calix is subject to change when it is deposited into films/membranes,

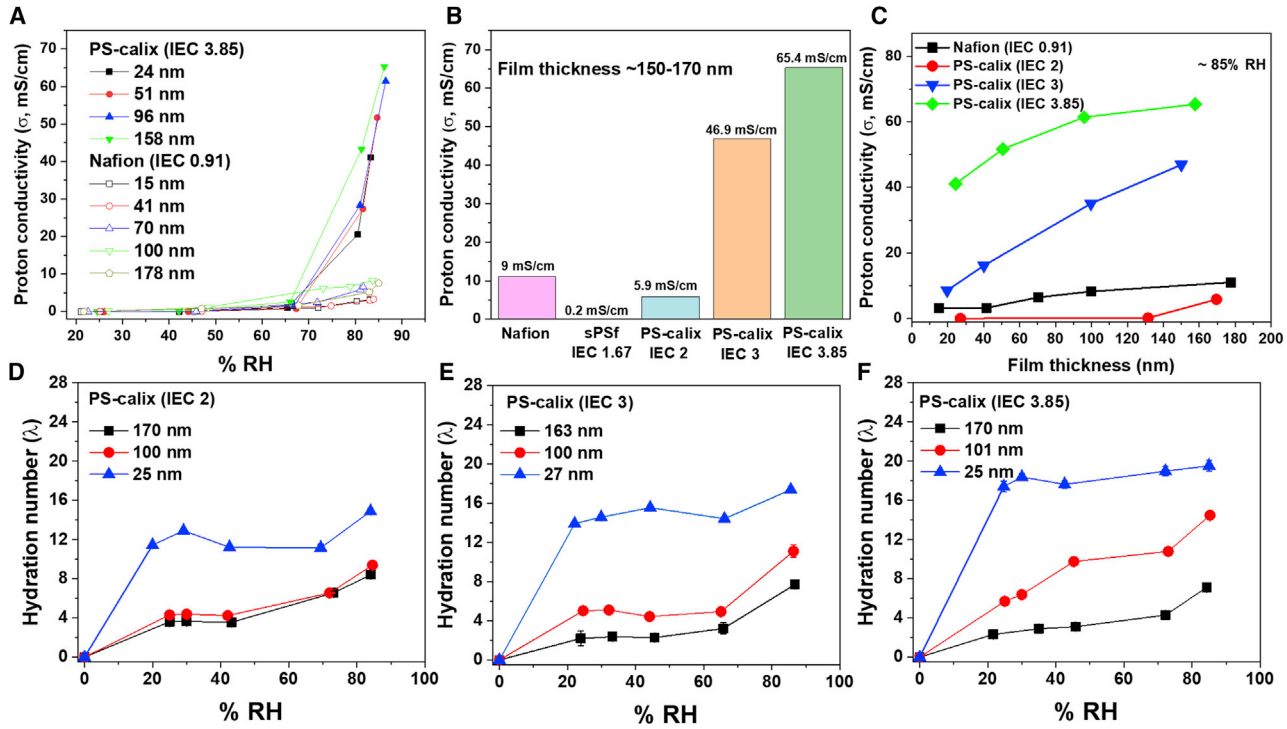

Figure 2. Proton conductivity and water uptake of ionomer thin films

(A) Comparison of proton conductivity (σ) of PS-calix (IEC 3.85) and Nafion as a function of %RH.

(B) Proton conductivity of ~150- to 170-nm-thick films of Nafion, sPSf, and PS-calix as a function of IEC at 85% RH.

(C) Effect of film thickness on proton conductivity of PS-calix and Nafion at ~85% RH.

(D–F) Hydration numbers (λ as moles of sorbed H_2O per mole of $–SO_3H$) of ~25- to 170-nm-thick films of PS-calix with IECs 2 (D), 3 (E), and 3.85 (F) as a function of film thickness and %RH. The measurements were all performed at room temperature. The λ values were bare-crystal-water-sorption corrected and plotted. The error bars are calculated based on the standard deviations.

exposed to humidity (plasticizing/antiplasticizing effects), and/or subjected to interfacial interactions.

Ionic conductivity and water uptake

Figures 2A–2C show the ion conduction performance of sub-micrometer-thick films of PS-calix in comparison with Nafion and sPSf. We measured the conductivity of the films with thickness ranging between 15 and 170 nm and at varied relative humidity (%RH) conditions (please see Table S2, Figure S4, and relevant discussions in the supplemental information for EIS fitting details). For the entire thickness range studied, PS-calix films always showed ionic conductivity significantly higher than Nafion and sPSf films. For example, when the film thickness was ~160–170 nm, the conductivity was 65.4 mS/cm for the PS-calix (IEC 3.85) sample, while it was only 9 mS/cm for Nafion and 0.2 mS/cm for sPSf at 85% RH (Figure 2B). Moreover, in films with thicknesses comparable to ionomer-based binder layers (~15–20 nm thick), the conductivity of PS-calix (IEC 3.85) film (41.1 mS/cm) was ~13 times higher than that of Nafion (3.3 mS/cm) (Figure 2C) and ~3 orders of magnitude higher than that of sPSf (0.01 mS/cm). These results showed a high potential of PS-calix as a catalyst-binding ionomer. We saw an IEC-dependent increase in the proton conductivity of PS-calix films (Figures 2B and 2C). But interestingly, at high IEC (3.85), the ionic conductivity of PS-calix films was not very sensitive to film thickness, i.e., proton conductivity did not drop significantly as the films became thinner (Figure 2C). This high-IEC variant of PS-calix was also not water soluble and, therefore, was useful for practical

water-mediated ion transport. These characteristics make PS-calix an attractive alternative to Nafion, the typical ionomer, which often suffers from low conductivity in low-thickness films.[24,25] Another interesting observation was that, at similar IEC values, PS-calix (5.9 mS/cm) was a better proton conductor than sPSf (0.2 mS/cm) (Figure 2B), a well-accepted hydrocarbon-based ionomer, which conducts protons as efficiently as Nafion in bulk membranes but fails to conduct protons efficiently in sub-micrometer-thick layers.[33,35,46,53]

We looked into the water uptake of these ionomer samples (Figures 2D–2F). Water uptake of PS-calix films increased with the increase in IEC, which is a rational trend due to the increased degree of sulfonation. Interestingly, an ~170-nm-thick Nafion film ($\lambda \sim 9$, Figure S5) absorbed more water than a PS-calix (IEC 3.85) film ($\lambda \sim 7$, Figure 2F), but the Nafion film showed proton conductivity (9 mS/cm) lower than that of PS-calix film (65 mS/cm) (Figure 2B). Such higher water uptake by thinner films and uncorrelated water uptake-conductivity trends have repeatedly been seen earlier for Nafion[37,38] and many other ionomers[24,25,35,40,111] in sub-micrometer-thick films. Several reasons have been identified, but in general, the amount of water uptake was found to be less important than how the sorbed water molecules segregate to form ionic domains/ion channels/ion transport pathways. We also saw that PS-calix film (IEC 3.85) had water uptake only 1.28 times higher than Nafion in ~25-nm-thick films (Figures 2F and S5). However, the proton conductivity of PS-calix was much stronger than that of Nafion (14 times) (Figures 2A–2C) at this thickness. This is why it may not be appropriate to attribute the higher ionic conductivity of the PS-calix films solely to higher water uptake. Rather, it likely suggests that the water molecules in PS-calix films are more efficient in conducting ions compared with Nafion films.

An important observation along that direction was the swelling of these ionomer films. At similar water uptake, the swelling of a PS-calix film was less than that of a Nafion film. The percentage swelling of an ~180-nm-thick film was ~13% for Nafion, but just 1.3% for PS-calix (based on CLSM analysis). This suggested that the macrocyclic hollow cavities within PS-calix were likely accommodating a large fraction of the upcoming water molecules without making the films swell much. In a typical scenario, protons hop across a network of water and $-SO_3H$ groups appended to the ionomers. But our prior working experience with macrocycle-based ionomers[24] made us hypothesize that in addition to this traditional pathway the water/ion translocation capability analogous to biological[59]/synthetic[79–81,85,90,94–96] ion channels may make a contribution to the unprecedentedly high proton conductivity of PS-calix, owing to the sub-nanometer-sized, sulfonated macrocyclic calix[4]arene features.

Water diffusion across ionomer films

In the quest to understand how the water molecules in PS-calix were more efficient in conducting ions, we lined up a proof showing that macrocycle-containing ionomers make water diffuse faster. Using DOSY NMR, we measured the water self-diffusion coefficient ($D_{self,\ water}$) within ~300-nm-thick, hydrated PS-calix and Nafion films (see Figure S6 and relevant section in the supplemental information for detailed experimental protocol). $D_{self,\ water}$ captures how fast or slow water diffuses under the influence of a negligible driving force (i.e., Brownian motion). $D_{self,\ water}$ of the Nafion film at 100% RH was 2.5×10^{-10} m^2/s, while the $D_{self,\ water}$ increased to 3.9×10^{-9} m^2/s for PS-calix (IEC 3) and 7.1×10^{-9} m^2/s for PS-calix (IEC 3.85) films with similar thicknesses (Figure 3A). Simultaneous observation of very high $D_{self,\ water}$ (water transport) and σ (proton conductivity) of PS-calix suggested that the macrocycle-containing ionomers likely have the capability to create unique and faster

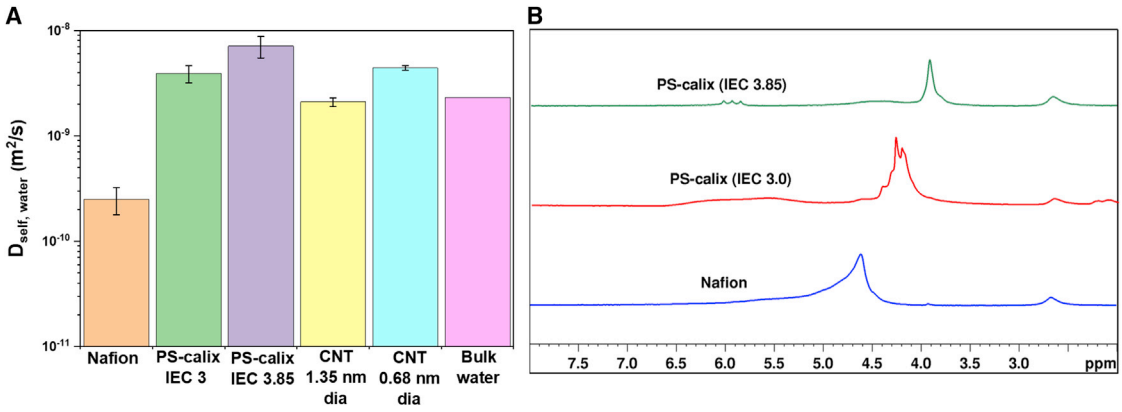

Figure 3. Water diffusion behavior within ionomer thin films

(A) Water self-diffusion coefficients ($D_{self, water}$) of Nafion, PS-calix (IEC 3, 3.85), CNTs with >1 nm and sub-nanometer diameters, and bulk water. Nafion and PS-calix data were obtained for ~300-nm-thick films at 100% RH using DOSY NMR for this work (error bars calculated based on standard deviations). CNT and bulk water data were taken from the literature for comparison.[91,112–115]

(B) ^{1}H NMR of ~300-nm-thick Nafion and PS-calix (IEC 3, 3.85) films.

water and ion-transport pathways, in agreement with our prior work.[24] Not only that, but in some cases, the values of $D_{self, water}$ in PS-calix films were even higher than what is reported for bulk water (2.3×10^{-9} m^2/s).[112–115] Using CNTs, Noy and colleagues[91] showed that "faster-than-bulk" water transport behavior can be achieved when the diameter of the CNT is narrowed down to sub-nanometer sizes (shown in Figure 3A for comparison). The sub-nanometer-size constrictions have also been found beneficial to make water move very fast through a range of natural (gramicidin A [4 Å])[35] and artificial channels,[79–84,116] as angstrom-scale conduits can compel water molecules to align into a single file (1D water wire) and enable their frictionless "slip" flow.[64,77] Noy and coworkers also showed that the sub-nanometer-sized CNTs conduct protons faster than their larger-than-1-nm counterparts.[90] From these works, they inferred that sub-nanometer-sized hydrophobic channels should enhance the proton transport rate due to the 1D water wire.[90] Our macrocycles in PS-calix also have similar features (sub-nanometer-sized cavities made of bridged aromatic rings, creating a hydrophobic interior and confining water into 1D sub-nanospace). While it is difficult to experimentally quantify the relative contributions of macrocycles and $-SO_3H$-water-based conventional proton hopping pathways (exterior to macrocyclic units) on the overall σ, in our previous work, we showed that a non-macrocycle-containing analog of a macrocycle-containing ionomer could have several orders of magnitude weaker proton conductivity.[24] We also showed the possible presence of H-bonded 1D water wires across macrocyclic calix[4]arene cavities in another ionomer via molecular dynamics (MD) simulations.[24] Furthermore, the water peak in ^{1}H NMR shifted to lower parts per million (ppm) and became narrower for PS-calix compared with Nafion in thin films at 100% RH (Figure 3B). This suggested improved mobility of protons and relatively looser H bonding of water molecules[50,117] in PS-calix, both of which are expected[63,118] within the hydrophobic interior of the sub-nanometer-sized macrocyclic cavities. All this evidence suggested that sub-nanometer-sized macrocycles in PS-calix, a missing feature in Nafion, may play an important role in making both water and proton transport faster in PS-calix films.

Depth-specific proton conduction behavior across ionomer films

We not only explored the overall proton conductivity but also explored the distribution of the proton conduction environment across ionomer thin films. This

measurement was critical, as the interactions near interfaces can predominantly control the properties across thin polymeric and biological systems.[30,40,41,47,119] In fact, interfacial interaction-induced substrate pinning is considered responsible for low water-ionomer mobility[41,47] and low ionic conductivity[30,40] of ionomer thin films. In our prior work,[30] we reported the distribution of the ionic conduction environment across Nafion thin films. In those films, we consistently saw a flat, very poor proton-conducting region spanning up to half of the film thickness, starting from the substrate interface. Similar observations (i.e., better ionomer-water mobility and ionic conductivity away from the interface) were reported by others via molecular simulation.[120] This suggested that if we can improve the interfacial ionic conductivity, we may be able to improve the overall ion conduction performance of the ionomer thin films. Interestingly, we found that PS-calix improved the interfacial ion conduction behavior (Figures 4A and 4B). We performed CLSM of photoacid stained Nafion and PS-calix films. The working mechanism of photoacid (8-Hydroxypyrene-1,3,6-trisulfonic acid trisodium salt, HPTS) and the strategy to obtain CLSM-derived proton conduction profile are discussed in our prior work[24] and in the supplemental information. Briefly, the photoacid shows ratiometric (green/blue) fluorescence (I_d/I_p), which increases when the ionic conductivity in a position within a film increases. Therefore, a higher I_d/I_p at a certain depth within a film indicates a more favorable proton conduction at that location within the film. Figures 4A and 4B show the proton conduction profile (I_d/I_p) across ~140- to 280-nm-thick Nafion and PS-calix (IEC 3.85) films. We saw that the proton conduction property (I_d/I_p) at the substrate interface significantly improved when Nafion was replaced by PS-calix. The I_d/I_p at the substrate interface for ~140-nm-thick Nafion film was 0.09, while it was 0.26 for PS-calix film with similar thickness (Figure 4A). The ion conduction at the air interface also significantly improved when PS-calix was used ($I_d/I_p \sim 0.58$ [PS-calix] and 0.17 [Nafion] for ~140-nm-thick films, Figure 4A). A similar 3–4 times improvement in interfacial proton conductivity (both substrate and air interface) was experienced with thicker (280-nm-thick) PS-calix films (compared with Nafion), achieving an I_d/I_p value as high as 0.9 at the air interface of the PS-calix film (Figure 4B). The corresponding xy-plane images (pseudo-colored) are shown in Figure S7. The improvement of interfacial proton conductivity, especially at the substrate interface, is a major milestone achieved. Also, the improvement in conduction at the substrate interface (from I_d/I_p) may be the reason we consistently saw high overall proton conductivity (σ) from PS-calix (IEC 3.85) samples irrespective of film thickness.

The origin of improved interfacial ionic conduction

Alterations of interfacial interactions may modulate the interfacial proton conduction properties, as seen in the CLSM results (Figures 4A and 4B). Here, we measured the overall viscoelastic properties and depth-specific elemental composition across ionomer films to assess the extent of interfacial interactions and rationalize the improvement in interfacial proton conduction behavior of PS-calix films. Using SEM/EDX, we made some interesting observations on the sulfur content (%S, Figures 4C and 4D) and sulfur-to-carbon ratio (Figures 4E and 4F) at different depths within Nafion and PS-calix films. In general, the substrate interface was more S rich than the air interface of Nafion films (e.g., %S 5.63% [substrate] vs. 3.04% [air] for 150-nm-thick Nafion film). In contrast, PS-calix films had a smaller %S near the substrate interface (1.14%) compared with the air interface (3.29%). Moreover, a higher accumulation of $–SO_3H$ next to the substrate was evident for Nafion films, as it contained higher %S than PS-calix films at the substrate interface (%S 5.63% [Nafion] and 1.14% [PS-calix] in 150-nm-thick films). The element S is a constituent of $–SO_3H$ groups that is supposed to conduct protons. However, if the $–SO_3H$ groups at the substrate interface bind intensely with the functionalities of the substrate (–SiOH

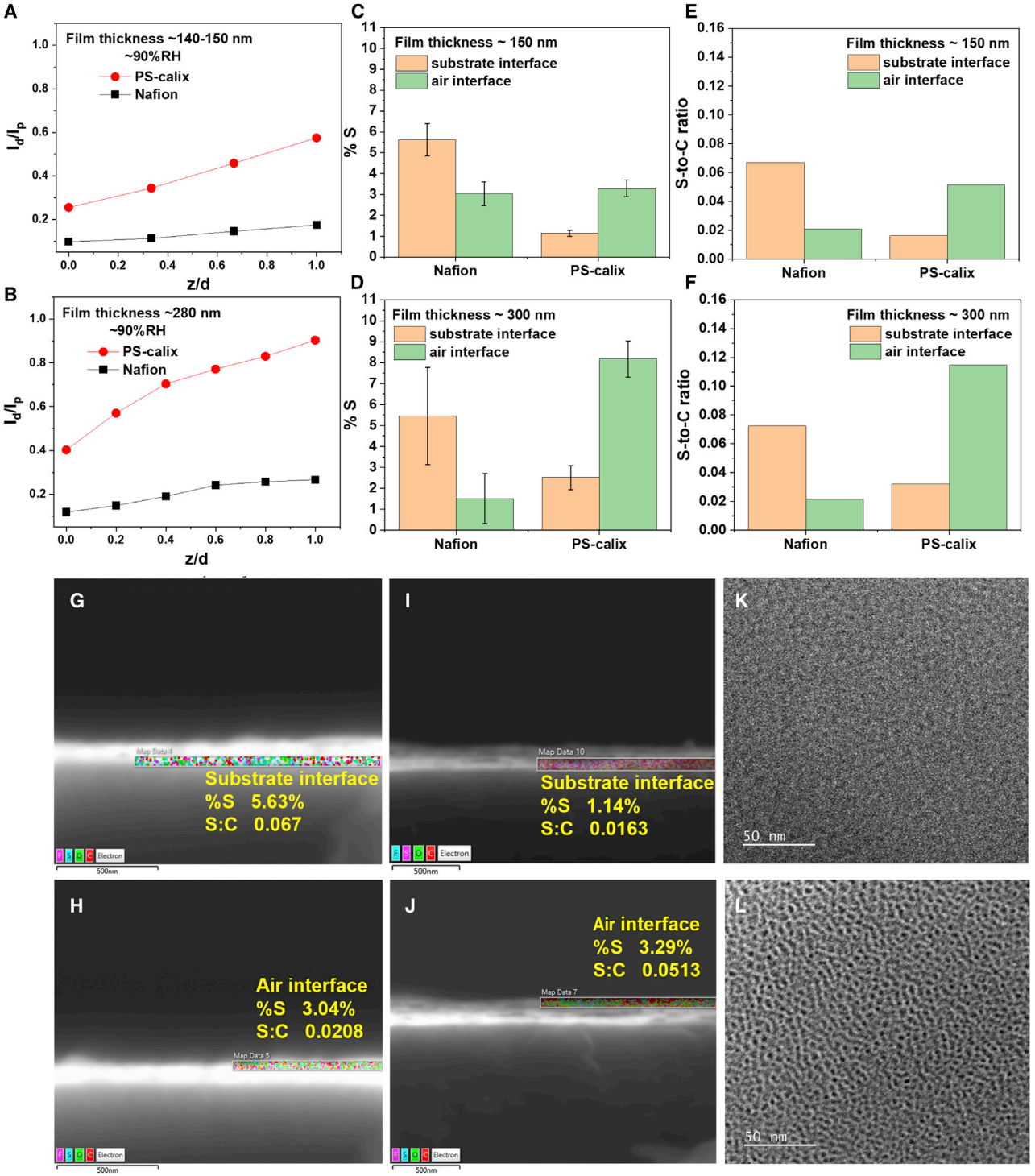

Figure 4. Depth-specific ion conduction behavior, elemental distribution at interfaces, and phase segregation within ionomer films

(A and B) Proton conduction profile (I_d/I_p) across (A) ~140- to 150-nm-thick and (B) ~280-nm-thick PS-calix (IEC 3.85) and Nafion films measured using CLSM. The term z/d represents thickness-normalized distance within a film starting from the substrate interface. The value of z/d will thus be 0 and 1 at the substrate and air interfaces, respectively.

(C–F) The %S (C and D, with error bars based on standard deviations) and the S-to-C ratio (E and F) at air and substrate interfaces of ~150-nm-thick (C and E) and 300-nm-thick (D and F) Nafion and PS-calix films.

Figure 4. *Continued*
(G–J) Cross-sectional SEM/EDX images of ~150-nm-thick Nafion (G and H) and PS-calix (IEC 3.85) (I and J) films showing elemental mapping at the substrate and air interfaces (boxed regions). The elements F, S, O, and C are presented by pink, cyan, green, and red colors, respectively.
(K and L) TEM images of ~50-nm-thick Nafion (K) and PS-calix (IEC 3.85) (L) films. Here, the dark and bright regions correspond to the hydrophilic ionic domains and hydrophobic phases, respectively. TEM samples were stained with Pb^{2+} ions.

here) and interfacial water molecules, even a high percentage of interfacial $–SO_3H$ can be detrimental to proton conduction. The intense binding can lead to a higher stiffness, which was evident from the higher storage modulus of Nafion films compared with PS-calix films (519.36 MPa [Nafion] vs. 237.29 MPa [PS-calix] at 90% RH, 300-nm-thick films). The storage and loss moduli of the ionomer films, measured using CR-AFM and an *in situ* humidity chamber (Figure S8), are shown in Table S3.

The side chain of PS-calix is bulky due to the presence of calix[4]arene units in addition to the phenyl groups. Such bulky side chains of PS-calix can exert steric hindrance on the side chains of neighboring repeat units. As a result, the flexible backbone of PS-calix may adopt a non-linear conformation, where the side chain (and its $–SO_3H$ groups) is less likely to line up along a single straight line. If such non-linear chains of PS-calix reach next to the substrate interface, they should have a smaller number of points of contact with the substrate as compared to Nafion, which aligns its backbone parallel to the substrate and directs its side chains toward the substrate, initiating sticky interfacial interactions. The weaker interfacial interactions corroborated with the smaller %S near the substrate interface of PS-calix films (Figures 4I and 4J) compared with Nafion films (Figures 4G and 4H).

Overall, both the SEM/EDX and the CR-AFM data greatly supported our proton conduction profiles (CLSM), where the PS-calix films exhibited 3 times better proton conduction near the substrate interface compared with Nafion films at the same region (Figures 4A and 4B). These results pointed out how strongly the substrate interface influences the overall properties of ionomer thin films and the need to understand the phenomena occurring at the substrate interface.

In contrast, being away from the substrate interface, the air interfaces of the films were relatively free of undesired interfacial interactions. Thus, the $–SO_3H$ groups at film-air interfaces were able to conduct protons more effectively (as seen in Figures 4A and 4B). It can, therefore, be inferred that the high proton conductivity at the air interface of PS-calix films was a combined effect of high %S and weak interfacial interactions. The high proton conductivity across the film was also supported by better hydrophilic-hydrophobic phase segregation observed in the TEM image of PS-calix film (Figure 4L, dark regions, ionic domains; bright regions, hydrophobic domains). The higher degree of phase mixing (i.e., poor dark-light phase contrast) in Nafion films (Figure 4K), on the other hand, was in agreement with prior works of us and others.[20,37]

Ionomer-catalyst mixed layer

Observing the high thin-film conductivity of PS-calix, we decided to explore the dispersion and conduction behavior of ionomers in the presence of a catalyst (Pt nanoparticles with ~3 nm diameter). We, therefore, made spin-coated films containing two components of typical catalyst inks, ionomer (Nafion or PS-calix) and catalyst (carbon was not included), and performed the elemental mapping of the films (Figures 5A–5J) using TEM/EDX. The TEM/EDX did not show any evidence of aggregation of Pt nanoparticles (Figure 5A) or PS-calix (Figures 5B–5D) in the mixed films. Rather, the Pt nanoparticles were uniformly dispersed within the PS-calix matrix. This is a desired property of a good catalyst ink.[21,121] More interestingly, the Pt

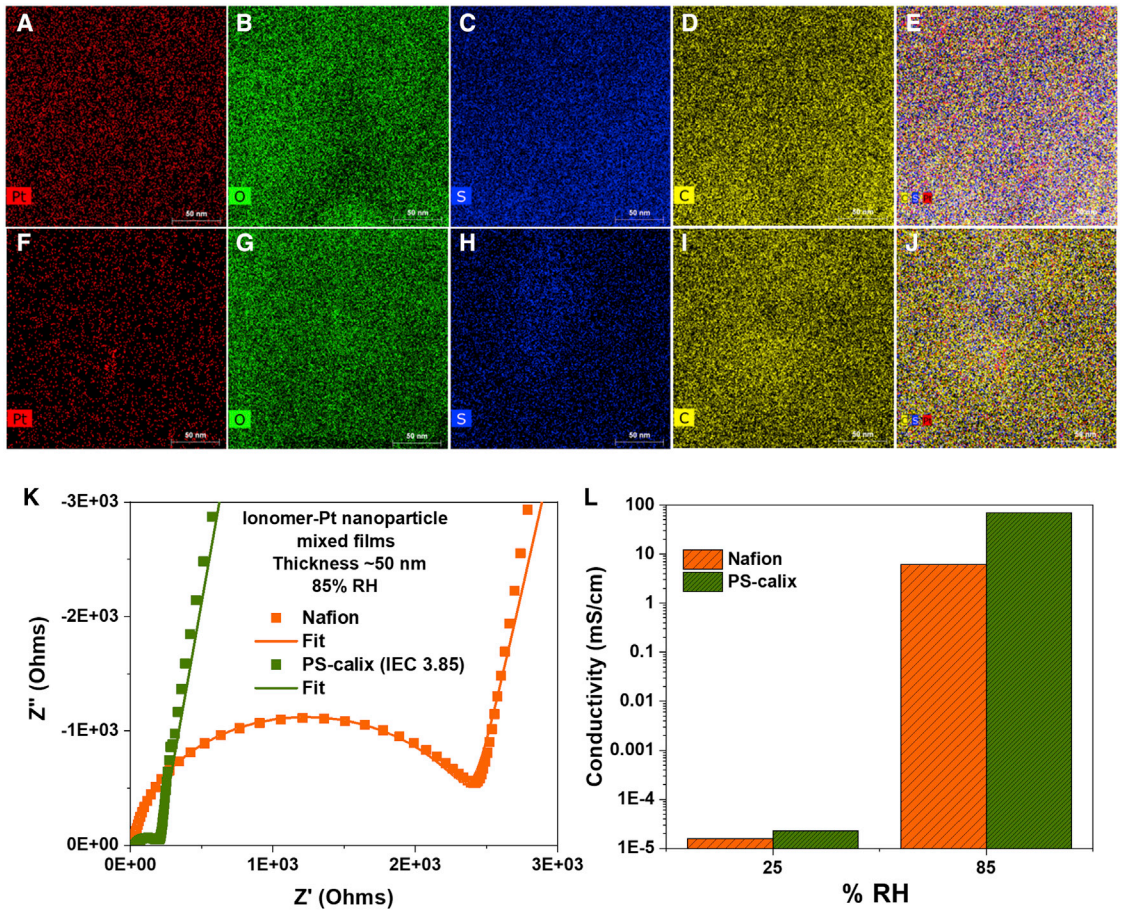

Figure 5. PS-calix-Pt nanoparticle mixed-layer performance

(A–E) TEM/EDX elemental maps (Pt, O, S, and C [A, B, C, and D, respectively] and overlay [E]) of an ~50-nm-thick PS-calix (IEC 3.85) film in which Pt nanoparticles were dispersed.

(F–J) TEM/EDX elemental maps (Pt, O, S, and C [F, G, H, and I, respectively] and overlay [J]) of an ~50-nm-thick Nafion film in which Pt nanoparticles were dispersed. Scale bars, 50 nm.

(K) Impedance spectra of mixed thin films containing Nafion or PS-calix with Pt nanoparticles at 85% RH.

(L) Conductivity values of the same samples at 25% and 85% RH. The thickness of the films was ~50 nm, and the diameter of the Pt nanoparticles was ~3 nm. The mass ratio of ionomer to Pt nanoparticles in the mixed suspension used to make the films was 10:0.013.

nanoparticles were more visible in the overlaid TEM/EDX images, suggesting that the catalyst particles were less masked by ionomer chains in PS calix-Pt nanoparticle mixed systems (Figure 5E) compared with Nafion-based ones (Figure 5J). The considerably smaller overlap of ionomer and catalyst in PS-calix-Pt systems was also evident from the Pt/C (w/w) ratio (0.015 [PS-calix] and 0.0025 [Nafion]) obtained from the TEM/EDX images. This observation agrees with what the literature has reported on Nafion-based catalyst inks, where the Nafion chains are shown to adsorb on the catalyst active sites via interaction between $–SO_3H$ (ionomer) and Pt. In fact, the $–SO_3H$ groups on the long and flexible side chains are shown to be more prone to adsorb on Pt surfaces.[52] Such coverage blocks the catalyst active sites, impedes the O_2 transport to those sites, and is thus detrimental to the ORR. Compared with Nafion, the side chains of PS-calix are bulky (due to calix[4]arene units) and subject to more steric hindrance with respect to the neighboring ones. Such effects may prevent $–SO_3H$ at neighboring calix[4]arene units from lining up toward Pt. This suggested a milder interaction between $–SO_3H$ of PS-calix (unlike Nafion) with Pt.

Also, a concern often raised about polyaromatic ionomers[46,122,123] is that their benzene rings may adsorb on Pt. Based on the highly exposed Pt surfaces in the ionomer matrix (Figure 4E), it can be inferred that the benzene-Pt interactions may not be that aggressive in the case of PS-calix. This could be attributed to the non-planar configuration of benzene ring-based macrocycles, which may prevent the positioning of benzene rings parallel to the substrate and potentially minimize the area of contact of the ionomer with Pt. Such mild interaction may also be the reason we saw better interfacial proton conduction in the CLSM study of PS-calix films on glass (SiO_2) surfaces (Figures 4A and 4B). The low blockage of catalyst active sites along with the intrinsic open structure of macrocycles with appropriate pore size[124] may make gas transport to Pt-active sites facile. In that respect, macrocycle-based ionomers can satisfy a critical design need of ionomer binder layers and show an effective way to address gas transport limitation, increase catalyst active site utilization, and thereby increase ORR efficiency.

We also found that, not only in simple thin films on substrates but also in ionomer-catalyst mixed systems, PS-calix offered higher proton conductivity compared with Nafion (Figures 5K and 5L). At 85% RH, PS-calix-Pt mixed films showed a conductivity of 69.58 mS/cm, while it was 6.12 mS/cm for Nafion-Pt-based ones. With the contributions from both (1) the traditional surface proton hopping pathways (exterior to macrocyclic units) and (2) the open macrocyclic features (facilitating the formation of exposed pathways), PS-calix offered a high thin-film proton conductivity that makes PS-calix a strong ionomer candidate to address both ion and gas transport limitations at ionomer-catalyst interfaces of PEMFC cathodes.

In summary, here, we report a new class of ionomer (PS-calix) having a styrene-based backbone and sulfonated calix[4]arene-based pendants. Leveraging its hollow, sub-nanometer-sized macrocyclic cavities, PS-calix was able to form unique and faster water and ion transport pathways and enhanced the proton conductivity in sub-micrometer-thick ionomer films, a system mimicking the ionomer binder layers on PEMFC electrodes. Nafion and sPSf, the two most promising proton conductors in bulk membrane separators, conduct protons poorly in such thin systems. But PS-calix (IEC 3.85) showed proton conductivity (41.1 mS/cm) ~13 times higher than Nafion and ~3 orders of magnitude higher than sPSf. The exceedingly high proton conductivity over Nafion was attributed to an order of magnitude faster water diffusion across PS-calix films. The water transport in PS-calix films was even faster than in bulk water. This faster-than-bulk water transport in thin films was likely mediated by the 1D water wires across macrocyclic cavities, a feature missing in Nafion. We simultaneously investigated the distribution of the ion conduction environment and elemental composition at different interfaces of ionomer films. The lower $–SO_3H$ accumulation and thus reduced interfacial interactions next to the substrate interface elevated the ion conduction next to the substrate interface as well as across the entire PS-calix film. This was in contrast with Nafion, which stiffened as a higher percentage of $–SO_3H$ localized near the substrate and interacted, making Nafion films suffer from poor proton conductivity next to the substrate interface. PS-calix outperformed Nafion even when it interfaced with Pt-catalyst in a mixed film and offered an order of magnitude higher proton conductivity than a Nafion-Pt-based system. In addition to addressing ion transport limitation, PS-calix showed the potential to alleviate gas transport limitations by masking the catalyst nanoparticles less than Nafion. Overall, the elevated ion and gas transport potentials of PS-calix at nanothin catalyst interfaces open new avenues to advance ionomer design principles. By guiding the water and ions through appropriate

sizes of constrictions, we can construct effective ionomer-catalyst interfaces/catalyst binder layers for fuel cells, electrolyzers, batteries, and many other sustainable energy technologies.

EXPERIMENTAL PROCEDURES

Resource availability

Lead contact

Further information and requests for resources should be directed to and will be fulfilled by the lead contact, Shudipto K. Dishari (sdishari2@unl.edu).

Materials availability

All unique and stable reagents generated in this study will be made available from the lead contact with a completed Materials Transfer Agreement.

Data and code availability

Data generated and used in this study are provided in this article and the supplemental information. Additional data are available from the lead contact (sdishari2@unl.edu) upon reasonable request. The article does not report any original code.

Synthesis and analytical characterization of 25,27-bis-(4-vinylbenzyloxy)-26,28-dihydroxycalix[4]arene (monomer 1)

A suspension of anhydrous sodium carbonate (4.78 g, 45.08 mmol) and calix[4]arene (9.43 g, 22.21 mmol) in dry acetonitrile (CH_3CN, 200 mL) was stirred under a N_2 atmosphere for 5 min. After that, 4-vinylbenzyl chloride (6.88 g, 45.08 mmol) and 20 μL of nitrobenzene was added. The reaction mixture was stirred vigorously at 70°C and refluxed under an N_2 atmosphere for 7 days. After cooling, the solvent was removed by vacuum evaporation. The residue was treated with 100 mL of aq HCl solution (5 vol %) and extracted using $CHCl_3$. After vacuum evaporation of the solvent ($CHCl_3$), recrystallization of the residue using $CHCl_3$-*n*-butanol gave monomer 1 as a white solid (11.67 g, yield 80%). Chemical formula: $C_{46}H_{40}O_4$ (MW 656.82 g/mol). Anal. calcd. for $C_{46}H_{40}O_4$: C 84.12; H 6.14; O 9.74. Found: C 84.14; H 6.26; O 9.60. ^{1}HNMR ($CDCl_3$, 400 MHz): δ_H = 7.82 (2H, Ar-**OH**), 7.64–7.40 (4H each, d each, Ar-**H** of vinyl benzene), 7.07 (4H, s, Ar**H** of calix unit), 6.89 (4H, s, Ar**H** of calix unit), 6.75 (4H, s, Ar**H** of calix unit), 6.66 (2H, dd, each –C**H**=CH_2), 5.81 (1H each, d, –CH=C**H**H), 5.28 (1H each, d, –CH=CH**H**), 5.06 (4H, s, ArO**CH$_2$**Ar), 4.34 (4H, d, Ar**CH$_2$**Ar), 3.38 (4H, d, Ar**CH$_2$**Ar). ^{13}C NMR ($CDCl_3$, TMS, 100 MHz): 153.37 (–OH-**C** of calix, 2C), 151.9 (–*O*–**C** of calix, 2C), 137.33 (–**C**H=CH_2, 2C), 136.37 (**Ar**, 4C), 133.20 (**Ar**, 4C), 129.05–125.46 (**Ar**, 20C), 118.96 (**Ar**, 4C), 114.14 (–CH=**C**H$_2$, 2C), 78.12 (–*O*–**C**–Ar, 2C), 31.44 (Ar–**C**H$_2$–Ar, 4C).

Synthesis of PS-calixn

Monomer 1 (1 g, 1.52 mmol) and benzoyl peroxide (BPO; 3.63 mg, 0.015 mmol) were dissolved in 10 mL of dry THF and stirred at 60°C under a N_2 atmosphere for 48 h. The reaction mixture was then cooled down to room temperature and quenched subsequently in an ice bath with stirring. The residue was dissolved in a minimum amount of dichloromethane and precipitated in methanol. The precipitation process was repeated twice to make the polymer free of unreacted monomers. After drying in a vacuum oven at 65°C, the polymer PS-calixn was obtained as a white solid (0.4 g, yield 40%). Chemical formula: $(C_{46}H_{40}O_4)_n$ (MW of repeat unit 656.82 g/mol). Molecular weight (M_n 11,450 g/mol, PDI 2.13). Anal. calcd. for $(C_{46}H_{40}O_4)_n$: C 84.12; H 6.14; O 9.74. Found: C 82.84; H 7.46; O 9.70. ^{1}HNMR ($CDCl_3$, 400 MHz): δ_H = 8.43 (2H, s, Ar**OH**), 7.82–7.41 (6H, br, Ar**H**), 7.08–6.75 (14H, br, Ar**H**),

4.86 (4H, br, Ar-OC**H**$_2$-Ar), 4.35 (4H, d, ArC**H**$_2$Ar), 3.35 (4H, d, ArC**H**$_2$Ar), 1.27–1.12 (6H, br, aliphatic **H**).

Synthesis of acetyl sulfate (sulfonation reagent)

The acetyl sulfate was freshly prepared prior to each sulfonation reaction. To do so, first, dichloromethane (5 mL) and acetic anhydride (1 mL, 9.70 mmol) were mixed for 3 h under an inert N_2 atmosphere. The solution was then cooled down to 0 °C, and 95% sulfuric acid (0.9 mL, 16.65 mmol) was added. This reaction mixture was stirred until a homogeneous and clear solution was obtained at room temperature. About 8 mL of acetyl sulfate was obtained following this procedure.

Sulfonation reaction for PS-calix (IECs 2, 3, 3.85)

PS-calixn (1 g) was dissolved in 5 mL of dichloromethane in a three-neck round-bottom flask equipped with a stirrer, thermometer, and dropping funnel. The flask containing the solution was heated to 40 °C to obtain a clear homogeneous solution of PS-calixn and then purged with N_2 for 30 min. A freshly prepared acetyl sulfate solution was added dropwise using a dropping funnel. The ratio of PS-calixn to acetyl sulfate was maintained at 1:1, 1:2, and 1:2.5 to yield PS-calix ionomers with IECs of 2, 3, and 3.85, respectively. The reaction mixture was maintained at 0 °C under stirring for 5 h. The reaction mixture was filtered, and the residue was dissolved in methanol. The methanol solution was washed with NaOH solution (10% aqueous) to neutralize the excess acetyl sulfate and subsequently dialyzed (MWCO of the dialysis membrane <6,000) for 3 days and dried in a vacuum oven at 50 °C overnight. Finally, light gray powders were obtained (0.12 g, 10% [IEC 2]; 0.16 g, 12% [IEC 3]; 0.18 g, 12% [IEC 3.85]). Molecular weight (M_n 12,120 g/mol, PDI 2.87 [IEC 2]; M_n 12,880 g/mol, PDI 3.2 [IEC 3]; M_n 13,001 g/mol, PDI 3.68 [IEC 3.85]). FTIR (cm^{-1}): 3,340–3,363 cm^{-1} (–OH stretching), 2,924 cm^{-1} (sp^2 aromatic C–H stretching), 1,581 cm^{-1} (aromatic C=C stretching), 1,151, 1,090 cm^{-1} (–S=O asymmetric and symmetric stretching), 903 cm^{-1} (S–O stretching), 683 cm^{-1} (C–S stretching). See the supplemental information for further details of materials, methods, and characterization.

SUPPLEMENTAL INFORMATION

Supplemental information can be found online at https://doi.org/10.1016/j.xcrp.2023.101282.

ACKNOWLEDGMENTS

The research was primarily supported by a National Science Foundation (NSF) CAREER Award (NSF-DMR 1750040) (polymeric ionomer synthesis, proton conductivity, water uptake, mechanical properties, distribution of ionic conduction environment and chemical mapping across thin films, interfacial properties of ionomer-catalyst mixed systems). The water diffusion studies across macrocycle-containing films were supported by the US Department of Energy (DOE), Office of Science, Basic Energy Sciences (BES), under Award DE-SC0020336. S.K.D. acknowledges support from the NSF CAREER Award for purchasing the EIS instrument. S.C., E.Z., S.F., and O.A.O. acknowledge partial support from the NSF (NSF-DMR 1750040), DOE (DE-SC0020336), and Nebraska Center for Energy Sciences Research, University of Nebraska-Lincoln (NCESR). CLSM images were taken at the Microscopy Core Facility of the Nebraska Center for Biotechnology. We acknowledge the UNL Molecular Analysis and Characterization (MAC) Facility for NMR work and acknowledge the Nebraska Center for Integrated Biomolecular Communication (NCIBC). A helium recovery system supporting the NMR spectrometers was purchased with support from

the NCIBC Systems Biology Core (NIH NIGMS P20 GM 113126). Part of this research (DSC, TGA, SE, TEM, SEM/EDX) was performed in the Nebraska Nanoscale Facility: National Nanotechnology Coordinated Infrastructure and the Nebraska Center for Materials and Nanoscience, which are supported by the NSF under Award ECS 2025298, and the Nebraska Research Initiative. The authors thank the Nano-Engineering Research Core Facility (NERCF) at UNL for CRFM studies of ionomeric materials.

AUTHOR CONTRIBUTIONS

S.K.D. conceived the idea of a macrocycle-based ionomer design and conceptualized the project. S.C. performed the synthesis of PS-calix. S.C. and K.R. performed the chemical characterization (TGA, DSC, NMR, GPC, elemental analysis) of PS-calix ionomers and their precursor molecules. S.K.D., O.A.O., and E.Z. designed the experiments together to unravel the distributed, interfacial, and thin-film properties of ionomers. O.A.O., E.Z., K.R., S.F., M.M., and A.S. executed the plan by performing EIS, QCM, CLSM, SEM/EDX, TEM, and DOSY NMR experiments. O.A.O., E.Z., K.R., and S.C. contributed with S.K.D. to data compilation, data analysis, and writing the manuscript. All the authors reviewed the manuscript.

DECLARATION OF INTERESTS

A PCT application titled "Ionomers with Macrocyclic Moieties for Ion Conductivity and Permselectivity" (PCT/US21/70,432) has been filed by NUtech Ventures, the technology transfer affiliate of the University of Nebraska-Lincoln. S.K.D. is the inventor on this patent.

INCLUSION AND DIVERSITY

We support inclusive, diverse, and equitable conduct of research.

Received: November 8, 2022
Revised: December 17, 2022
Accepted: January 18, 2023
Published: February 8, 2023

REFERENCES

1. Roadmap to U.S. Hydrogen Economy. https://www.energy.gov/sites/prod/files/2017/11/f46/FCTT_Roadmap_Nov_2017_FINAL.pdf.

2. Cullen, D.A., Neyerlin, K.C., Ahluwalia, R.K., Mukundan, R., More, K.L., Borup, R.L., Weber, A.Z., Myers, D.J., and Kusoglu, A. (2021). New roads and challenges for fuel cells in heavy-duty transportation. Nat. Energy *6*, 462–474. https://doi.org/10.1038/s41560-021-00775-z.

3. Kongkanand, A., and Mathias, M.F. (2016). The priority and challenge of high-power performance of low-platinum proton-exchange membrane fuel cells. J. Phys. Chem. Lett. *7*, 1127–1137. https://doi.org/10.1021/acs.jpclett.6b00216.

4. Jiao, K., Xuan, J., Du, Q., Bao, Z., Xie, B., Wang, B., Zhao, Y., Fan, L., Wang, H., Hou, Z., et al. (2021). Designing the next generation of proton-exchange membrane fuel cells. Nature *595*, 361–369. https://doi.org/10.1038/s41586-021-03482-7.

5. Asano, N., Aoki, M., Suzuki, S., Miyatake, K., Uchida, H., and Watanabe, M. (2006). Aliphatic/aromatic polyimide ionomers as a proton conductive membrane for fuel cell applications. J. Am. Chem. Soc. *128*, 1762–1769. https://doi.org/10.1021/ja0571491.

6. Adamski, M., Peressin, N., and Holdcroft, S. (2021). On the evolution of sulfonated polyphenylenes as proton exchange membranes for fuel cells. Mater. Adv. *2*, 4966–5005. https://doi.org/10.1039/d1ma00511a.

7. Chang, Y., Mohanty, A.D., Smedley, S.B., Abu-Hakmeh, K., Lee, Y.H., Morgan, J.E., Hickner, M.A., Jang, S.S., Ryu, C.Y., and Bae, C. (2015). Effect of superacidic side chain structures on high conductivity aromatic polymer fuel cell membranes. Macromolecules *48*, 7117–7126. https://doi.org/10.1021/acs.macromol.5b01739.

8. Elabd, Y.A., and Hickner, M.A. (2011). Block copolymers for fuel cells. Macromolecules *44*, 1–11. https://doi.org/10.1021/ma101247c.

9. Yandrasits, M., Lindell, M., Schaberg, M., and Kurkowski, M. (2017). Increasing fuel cell efficiency by using ultra-low equivalent weight ionomers. Electrochem. Soc. Interface *26*, 49–53. https://doi.org/10.1149/2.F05171if.

10. Hickner, M.A., and Pivovar, B.S. (2005). The chemical and structural nature of proton exchange membrane fuel cell properties. Fuel Cell. *5*, 213–229. https://doi.org/10.1002/fuce.200400064.

11. Hickner, M.A., Ghassemi, H., Kim, Y.S., Einsla, B.R., and McGrath, J.E. (2004). Alternative polymer systems for proton exchange membranes (PEMs). Chem. Rev. *104*, 4587–4611. https://doi.org/10.1021/cr020711a.

12. Stamenkovic, V.R., Fowler, B., Mun, B.S., Wang, G., Ross, P.N., Lucas, C.A., and Marković, N.M. (2007). Improved oxygen reduction activity on Pt3Ni(111) via increased surface site availability. Science *315*, 493–497. https://doi.org/10.1126/science.1135941.

13. Li, D., Lv, H., Kang, Y., Markovic, N.M., and Stamenkovic, V.R. (2016). Progress in the

development of oxygen reduction reaction catalysts for low-temperature fuel cells. Annu. Rev. Chem. Biomol. Eng. *7*, 509–532. https://doi.org/10.1146/annurev-chembioeng-080615-034526.

14. Wu, G., More, K.L., Johnston, C.M., and Zelenay, P. (2011). High-performance electrocatalysts for oxygen reduction derived from polyaniline, iron, and cobalt. Science *332*, 443–447. https://doi.org/10.1126/science.1200832.

15. Wang, H., Wang, R., Sui, S., Sun, T., Yan, Y., and Du, S. (2021). Cathode design for proton exchange membrane fuel cells in automotive applications. Automot. Innov. *4*, 144–164. https://doi.org/10.1007/s42154-021-00148-y.

16. Avid, A., and Zenyuk, I.V. (2020). Ionic liquid modified Pt/C electrocatalysts for the oxygen reduction reaction in polymer electrolyte fuel cells. Meet. Abstr. *MA2020-02*, 2155. https://doi.org/10.1149/ma2020-02332155mtgabs.

17. Li, Y., Van Cleve, T., Sun, R., Gawas, R., Wang, G., Tang, M., Elabd, Y.A., Snyder, J., and Neyerlin, K.C. (2020). Modifying the electrocatalyst — ionomer interface via sulfonated poly(ionic liquid) block copolymers to enable high- performance polymer electrolyte fuel cells. ACS Energy Lett. *5*, 1726–1731. https://doi.org/10.1021/acsenergylett.0c00532.

18. Liu, C., Uchiyama, T., Ishihara, J., Yamamoto, K., Watanabe, T., Imai, H., Oshima, K., Sakurai, S., Inaba, M., and Uchimoto, Y. (2021). Operando X-ray absorption spectroscopic study on the effect of ionic liquid coverage upon the oxygen reduction reaction activity of Pd-core Pt-shell catalysts. Electrochemistry *89*, 31–35. https://doi.org/10.5796/ELECTROCHEMISTRY.20-00122.

19. Zhang, G., and Etzold, B.J.M. (2021). Emerging applications of solid catalysts with ionic liquid layer concept in electrocatalysis. Adv. Funct. Mater. *31*, 2010977–2011021. https://doi.org/10.1002/adfm.202010977.

20. Islam, M.N., Mansoor Basha, A.B., Kollath, V.,O., Soleymani, A.P., Jankovic, J., and Karan, K. (2022). Designing fuel cell catalyst support for superior catalytic activity and low mass-transport resistance. Nat. Commun. *13*, 6157–6211. https://doi.org/10.1038/s41467-022-33892-8.

21. Doo, G., Yuk, S., Lee, J.H., Choi, S., Lee, D.H., Lee, D.W., Hyun, J., Kwon, S.H., Lee, S.G., and Kim, H.T. (2020). Nano-scale control of the ionomer distribution by molecular masking of the Pt surface in PEMFCs. J. Mater. Chem. *8*, 13004–13013. https://doi.org/10.1039/c9ta14002f.

22. Pramounmat, N., Loney, C.N., Kim, C., Wiles, L., Ayers, K.E., Kusoglu, A., and Renner, J.N. (2019). Controlling the distribution of perfluorinated sulfonic acid ionomer with elastin-like polypeptide. ACS Appl. Mater. Interfaces *11*, 43649–43658. https://doi.org/10.1021/acsami.9b11160.

23. Zhou, Z.Y., Kang, X., Song, Y., and Chen, S. (2012). Ligand-mediated electrocatalytic activity of Pt nanoparticles for oxygen reduction reactions. J. Phys. Chem. C *116*, 10592–10598. https://doi.org/10.1021/jp300199x.

24. Chatterjee, S., Zamani, E., Farzin, S., Evazzade, I., Obewhere, O.A., Johnson, T.J., Alexandrov, V., and Dishari, S.K. (2022). Molecular-Level control over ionic conduction and ionic current direction by designing macrocycle-based ionomers. JACS Au *2*, 1144–1159. https://doi.org/10.1021/jacsau.2c00143.

25. Farzin, S., Johnson, T.J., Chatterjee, S., Zamani, E., and Dishari, S.K. (2020). Ionomers from kraft lignin for renewable energy applications. Front. Chem. *8*, 690–717. https://doi.org/10.3389/fchem.2020.00690.

26. Nagao, Y. (2017). Proton-conductivity enhancement in polymer thin films. Langmuir *33*, 12547–12558. https://doi.org/10.1021/acs.langmuir.7b01484.

27. Lim, K.H., Lee, A.S., Atanasov, V., Kerres, J., Park, E.J., Adhikari, S., Maurya, S., Manriquez, L.D., Jung, J., Fujimoto, C., et al. (2022). Protonated phosphonic acid electrodes for high power heavy-duty vehicle fuel cells. Nat. Energy *7*, 248–259. https://doi.org/10.1038/s41560-021-00971-x.

28. Venugopalan, G., Bhattacharya, D., Kole, S., Ysidron, C., Angelopoulou, P.P., Sakellariou, G., and Arges, C.G. (2021). Correlating high temperature thin film ionomer electrode binder properties to hydrogen pump polarization. Mater. Adv. *2*, 4228–4234. https://doi.org/10.1039/d1ma00208b.

29. Shrivastava, U.N., Fritzsche, H., and Karan, K. (2018). Interfacial and bulk water in ultrathin films of nafion, 3M PFSA , and 3M PFIA ionomers on a polycrystalline platinum surface. Macromolecules *51*, 9839–9849. https://doi.org/10.1021/acs.macromol.8b01240.

30. Farzin, S., Zamani, E., and Dishari, S.K. (2021). Unraveling depth-specific ionic conduction and stiffness behavior across ionomer thin films and bulk membranes. ACS Macro Lett. *10*, 791–798. https://doi.org/10.1021/acsmacrolett.1c00110.

31. Kusoglu, A., and Weber, A.Z. (2017). New insights into perfluorinated sulfonic-acid ionomers. Chem. Rev. *117*, 987–1104. https://doi.org/10.1021/acs.chemrev.6b00159.

32. Karan, K. (2019). Interesting facets of surface, interfacial, and bulk characteristics of perfluorinated ionomer films. Langmuir *35*, 13489–13520. https://doi.org/10.1021/acs.langmuir.8b03721.

33. Holdcroft, S. (2014). Fuel cell catalyst layers: a polymer science perspective. Chem. Mater. *26*, 381–393. https://doi.org/10.1021/cm401445h.

34. Modestino, M.A., Paul, D.K., Dishari, S., Petrina, S.A., Allen, F.I., Hickner, M.A., Karan, K., Segalman, R.A., and Weber, A.Z. (2013). Self-assembly and transport limitations in confined nafion films. Macromolecules *46*, 867–873. https://doi.org/10.1021/ma301999a.

35. Dishari, S. (2014). Current understanding of proton conduction in confined ionomeric systems. Postdoc J. *2*, 30–39. https://doi.org/10.14304/SURYA.JPR.V2N4.3.

36. Paul, D.K., McCreery, R., and Karan, K. (2014). Proton transport property in supported nafion nanothin films by electrochemical impedance spectroscopy. J. Electrochem. Soc. *161*, F1395–F1402. https://doi.org/10.1149/2.0571414jes.

37. Farzin, S., Sarella, A., Yandrasits, M.A., and Dishari, S.K. (2019). Fluorocarbon-based ionomers with single acid and multiacid side chains at nanothin interfaces. J. Phys. Chem. C *123*, 30871–30884. https://doi.org/10.1021/acs.jpcc.9b10015.

38. Kusoglu, A., Kushner, D., Paul, D.K., Karan, K., Hickner, M.A., and Weber, A.Z. (2014). Impact of substrate and processing on confinement of nafion thin films. Adv. Funct. Mater. *24*, 4763–4774. https://doi.org/10.1002/adfm.201304311.

39. Kushner, D.I., Kusoglu, A., Podraza, N.J., and Hickner, M.A. (2019). Substrate-dependent molecular and nanostructural orientation of nafion thin films. Adv. Funct. Mater. *29*, 1902699. https://doi.org/10.1002/adfm.201902699.

40. Dishari, S.K., and Hickner, M.A. (2013). Confinement and proton transfer in Nafion thin films. Macromolecules *46*, 413–421. https://doi.org/10.1021/ma3011137.

41. Dishari, S.K., and Hickner, M.A. (2012). Antiplasticization and water uptake of Nafion® thin films. ACS Macro Lett. *1*, 291–295. https://doi.org/10.1021/mz200169a.

42. Dura, J.A., Murthi, V.S., Hartman, M., Satija, S.K., and Majkrzak, C.F. (2009). Multilamellar interface structures in Nafion. Macromolecules *42*, 4769–4774. https://doi.org/10.1021/ma802823j.

43. DeCaluwe, S.C., Baker, A.M., Bhargava, P., Fischer, J.E., and Dura, J.A. (2018). Structure-property relationships at Nafion thin-film interfaces: thickness effects on hydration and anisotropic ion transport. Nano Energy *46*, 91–100. https://doi.org/10.1016/j.nanoen.2018.01.008.

44. Eastman, S.A., Kim, S., Page, K.A., Rowe, B.W., Kang, S., Soles, C.L., and Yager, K.G. (2012). Effect of confinement on structure, water solubility, and water transport in Nafion thin Films. Macromolecules *45*, 7920–7930. https://doi.org/10.1021/ma301289v.

45. Komini Babu, S., Chung, H.T., Zelenay, P., and Litster, S. (2016). Resolving electrode morphology's impact on platinum group metal-free cathode performance using nano-CT of 3D hierarchical pore and ionomer distribution. ACS Appl. Mater. Interfaces *8*, 32764–32777. https://doi.org/10.1021/acsami.6b08844.

46. Peron, J., Shi, Z., and Holdcroft, S. (2011). Hydrocarbon proton conducting polymers for fuel cell catalyst layers. Energy Environ. Sci. *4*, 1575–1591. https://doi.org/10.1039/c0ee00638f.

47. Dishari, S.K., Rumble, C.A., Maroncelli, M., Dura, J.A., and Hickner, M.A. (2018). Unraveling the complex hydration behavior of ionomers under thin film confinement. J. Phys. Chem. C *122*, 3471–3481. https://doi.org/10.1021/acsmacrolett.1c00110.

48. Luo, X., Kushner, D.I., Li, J., Park, E.J., Kim, Y.S., and Kusoglu, A. (2021). Anion exchange ionomers: impact of chemistry on thin-film

properties. Adv. Funct. Mater. *31*, 2008778–2008812. https://doi.org/10.1002/adfm.202008778.

49. Hsu, W.Y., and Gierke, T.D. (1983). Ion transport and clustering in nafion perfluorinated membranes. J. Membr. Sci. *13*, 307–326. https://doi.org/10.1016/S0376-7388(00)81563-X.

50. De Almeida, N.E., Paul, D.K., Karan, K., and Goward, G.R. (2015). 1H solid-state NMR study of nanothin Nafion films. J. Phys. Chem. C *119*, 1280–1285. https://doi.org/10.1021/jp5086747.

51. Poojary, S., Islam, M.N., Shrivastava, U.N., Roberts, E.P.L., and Karan, K. (2020). Transport and electrochemical interface properties of ionomers in low-pt loading catalyst layers: effect of ionomer equivalent weight and relative humidity. Molecules *25*, 3387–3414. https://doi.org/10.3390/molecules25153387.

52. Kodama, K., Motobayashi, K., Shinohara, A., Hasegawa, N., Kudo, K., Jinnouchi, R., Osawa, M., and Morimoto, Y. (2018). Effect of the side-chain structure of perfluoro-sulfonic acid ionomers on the oxygen reduction reaction on the surface of Pt. ACS Catal. *8*, 694–700. https://doi.org/10.1021/acscatal.7b03571.

53. Astill, T., Xie, Z., Shi, Z., Navessin, T., and Holdcroft, S. (2009). Factors influencing electrochemical properties and performance of hydrocarbon-based electrolyte PEMFC catalyst layers. J. Electrochem. Soc. *156*, B499–B508. https://doi.org/10.1149/1.3082119.

54. Budd, P.M., McKeown, N.B., and Fritsch, D. (2006). Polymers of intrinsic microporosity (PIMs): high free volume polymers for membrane applications. Macromol. Symp. *245–246*, 403–405. https://doi.org/10.1002/masy.200651356.

55. Ye, Y., Gong, L., Xiang, S., Zhang, Z., and Chen, B. (2020). Metal–organic frameworks as a versatile platform for proton conductors. Adv. Mater. *32*, 1907090. https://doi.org/10.1002/adma.201907090.

56. Geng, K., He, T., Liu, R., Dalapati, S., Tan, K.T., Li, Z., Tao, S., Gong, Y., Jiang, Q., and Jiang, D. (2020). Covalent organic frameworks: design, synthesis, and functions. Chem. Rev. *120*, 8814–8933. https://doi.org/10.1021/acs.chemrev.9b00550.

57. Zhang, Q., Dong, S., Shao, P., Zhu, Y., Mu, Z., Sheng, D., Zhang, T., Jiang, X., Shao, R., Ren, Z., et al. (2022). Covalent organic framework-based porous ionomers for high-performance fuel cells. Science *378*, 181–186. https://doi.org/10.1126/science.abm6304.

58. Shang, Z., Wycisk, R., and Pintauro, P. (2021). Electrospun composite proton-exchange and anion-exchange membranes for fuel cells. Energies *14*, 6709–6721. https://doi.org/10.3390/en14206709.

59. Akeson, M., and Deamer, D.W. (1991). Proton conductance by the gramicidin water wire. Model for proton conductance in the F1F0 ATPases? Biophys. J. *60*, 101–109. https://doi.org/10.1016/S0006-3495(91)82034-3.

60. Baaden, M., Barboiu, M., Bill, R.M., Casanova, S., Chen, C.L., Conner, M., Freger, V., Gong, B., Góra, A., Hinds, B., et al. (2018). Structure and function of natural proteins for water transport: general discussion. Faraday Discuss *209*, 83–95. https://doi.org/10.1039/C8FD90019A.

61. Pfeffermann, J., Goessweiner-Mohr, N., and Pohl, P. (2021). The energetic barrier to single-file water flow through narrow channels. Biophys. Rev. *13*, 913–923. https://doi.org/10.1007/s12551-021-00875-w.

62. Epsztein, R., DuChanois, R.M., Ritt, C.L., Noy, A., and Elimelech, M. (2020). Towards single-species selectivity of membranes with subnanometre pores. Nat. Nanotechnol. *15*, 426–436. https://doi.org/10.1038/s41565-020-0713-6.

63. Wang, H., Yang, C., Wang, S., and Hu, S. (2022). Tunable ion transport through ultimately small channels. Advanced Membranes *2*, 100043–100112. https://doi.org/10.1016/j.advmem.2022.100043.

64. Song, W., and Kumar, M. (2019). Artificial water channels: toward and beyond desalination. Curr. Opin. Chem. Eng. *25*, 9–17. https://doi.org/10.1016/j.coche.2019.06.007.

65. Barboiu, M. (2012). Artificial water channels. Angew. Chem., Int. Ed. Engl. *51*, 11674–11676. https://doi.org/10.1002/anie.201205819.

66. Köfinger, J., Hummer, G., and Dellago, C. (2011). Single-file water in nanopores. Phys. Chem. Chem. Phys. *13*, 15403–15417. https://doi.org/10.1039/c1cp21086f.

67. Köfinger, J., Hummer, G., and Dellago, C. (2008). Macroscopically ordered water in nanopores. Proc. Natl. Acad. Sci. USA *105*, 13218–13222. https://doi.org/10.1073/pnas.0801448105.

68. Mann, D.J., and Halls, M.D. (2003). Water alignment and proton conduction inside carbon nanotubes. Phys. Rev. Lett. *90*, 195503. https://doi.org/10.1103/PhysRevLett.90.195503.

69. Majumder, M., Chopra, N., Andrews, R., and Hinds, B.J. (2005). Enhanced flow in carbon nanotubes. Nature *438*, 44. https://doi.org/10.1038/438044a.

70. Markowitz, M.A., Janout, V., Castner, D.G., and Regen, S.L. (1989). Perforated monolayers: design and synthesis of porous and cohesive monolayers from mercurated calix[n]arenes. J. Am. Chem. Soc. *111*, 8192–8200. https://doi.org/10.1021/ja00203a020.

71. Yu, G., and Chen, X. (2019). Host–guest chemistry in supramolecular theranostics. Theranostics *9*, 3041–3074. https://doi.org/10.7150/thno.31653.

72. Jie, K., Zhou, Y., Yao, Y., and Huang, F. (2015). Macrocyclic amphiphiles. Chem. Soc. Rev. *44*, 3568–3587. https://doi.org/10.1039/C4CS00390J.

73. Addonizio, C.J., Gates, B.D., and Webber, M.J. (2021). Supramolecular "click chemistry" for targeting in the body. Bioconjug. Chem. *32*, 1935–1946. https://doi.org/10.1021/acs.bioconjchem.1c00326.

74. Zhang, Z., Sui, X., Li, P., Xie, G., Kong, X.Y., Xiao, K., Gao, L., Wen, L., and Jiang, L. (2017). Ultrathin and ion-selective janus membranes for high-performance Osmotic energy conversion. J. Am. Chem. Soc. *139*, 8905–8914. https://doi.org/10.1021/jacs.7b02794.

75. Liang, Y., Zhu, Y., Liu, C., Lee, K.R., Hung, W.S., Wang, Z., Li, Y., Elimelech, M., Jin, J., and Lin, S. (2020). Polyamide nanofiltration membrane with highly uniform sub-nanometre pores for sub-1 Å precision separation. Nat. Commun. *11*, 2015–2019. https://doi.org/10.1038/s41467-020-15771-2.

76. Elimelech, M., Phillip, W.A., and Phillip, W.A. (2011). The future of seawater and the environment. Science *333*, 712–717. https://doi.org/10.1126/science.1200488.

77. Faucher, S., Aluru, N., Bazant, M.Z., Blankschtein, D., Brozena, A.H., Cumings, J., Pedro De Souza, J., Elimelech, M., Epsztein, R., Fourkas, J.T., et al. (2019). Critical knowledge Gaps in mass transport through single-digit nanopores: a review and perspective. J. Phys. Chem. C *123*, 21309–21326. https://doi.org/10.1021/acs.jpcc.9b02178.

78. Choi, W., Ulissi, Z.W., Shimizu, S.F.E., Bellisario, D.O., Ellison, M.D., and Strano, M.S. (2013). Diameter-dependent ion transport through the interior of isolated single-walled carbon nanotubes. Nat. Commun. *4*, 2397–2398. https://doi.org/10.1038/ncomms3397.

79. Licsandru, E., Kocsis, I., Shen, Y.X., Murail, S., Legrand, Y.M., Van Der Lee, A., Tsai, D., Baaden, M., Kumar, M., and Barboiu, M. (2016). Salt-excluding artificial water channels exhibiting enhanced dipolar water and proton translocation. J. Am. Chem. Soc. *138*, 5403–5409. https://doi.org/10.1021/jacs.6b01811.

80. Barboiu, M., Le Duc, Y., Gilles, A., Cazade, P.A., Michau, M., Marie Legrand, Y., Van Der Lee, A., Coasne, B., Parvizi, P., Post, J., and Fyles, T. (2014). An artificial primitive mimic of the Gramicidin-A channel. Nat. Commun. *5*, 4142–4149. https://doi.org/10.1038/ncomms5142.

81. Zhou, X., Liu, G., Yamato, K., Shen, Y., Cheng, R., Wei, X., Bai, W., Gao, Y., Li, H., Liu, Y., et al. (2012). Self-assembling subnanometer pores with unusual mass-transport properties. Nat. Commun. *3*, 949–958. https://doi.org/10.1038/ncomms1949.

82. Zhao, H., Sheng, S., Hong, Y., and Zeng, H. (2014). Proton gradient-induced water transport mediated by water wires inside narrow aquapores of aquafoldamer molecules. J. Am. Chem. Soc. *136*, 14270–14276. https://doi.org/10.1021/ja5077537.

83. Shen, Y.X., Si, W., Erbakan, M., Decker, K., De Zorzi, R., Saboe, P.O., Kang, Y.J., Majd, S., Butler, P.J., Walz, T., et al. (2015). Highly permeable artificial water channels that can self-assemble into two-dimensional arrays. Proc. Natl. Acad. Sci. USA *112*, 9810–9815. https://doi.org/10.1073/pnas.1508575112.

84. Hu, X.B., Chen, Z., Tang, G., Hou, J.L., and Li, Z.T. (2012). Single-molecular artificial transmembrane water channels. J. Am. Chem.

Soc. *134*, 8384–8387. https://doi.org/10.1021/ja302292c.

85. Si, W., Chen, L., Hu, X.B., Tang, G., Chen, Z., Hou, J.L., and Li, Z.T. (2011). Selective artificial transmembrane channels for protons by formation of water wires. Angew. Chem., Int. Ed. Engl. *50*, 12564–12568. https://doi.org/10.1002/anie.201106857.

86. Li, X., Zhang, H., Hou, J., Ou, R., Zhu, Y., Zhao, C., Qian, T., Easton, C.D., Selomulya, C., Hill, M.R., and Wang, H. (2020). Sulfonated sub-1-nm metal-organic framework channels with ultrahigh proton selectivity. J. Am. Chem. Soc. *142*, 9827–9833. https://doi.org/10.1021/jacs.0c03554.

87. Porter, C.J., Werber, J.R., Zhong, M., Wilson, C.J., and Elimelech, M. (2020). Pathways and challenges for biomimetic desalination membranes with sub-nanometer channels. ACS Nano *14*, 10894–10916. https://doi.org/10.1021/acsnano.0c05753.

88. Chaturvedi, P., Moehring, N.K., Cheng, P., Vlassiouk, I., Boutilier, M.S.H., and Kidambi, P.R. (2022). Deconstructing proton transport through atomically thin monolayer CVD graphene membranes. J. Mater. Chem. *10*, 19797–19810. https://doi.org/10.1039/d2ta01737g.

89. Ruiz, L., Wu, Y., and Keten, S. (2015). Tailoring the water structure and transport in nanotubes with tunable interiors. Nanoscale *7*, 121–132. https://doi.org/10.1039/c4nr05407e.

90. Tunuguntla, R.H., Allen, F.I., Kim, K., Belliveau, A., and Noy, A. (2016). Ultrafast proton transport in sub-1-nm diameter carbon nanotube porins. Nat. Nanotechnol. *11*, 639–644. https://doi.org/10.1038/nnano.2016.43.

91. Tunuguntla, R.H., Henley, R.Y., Yao, Y.C., Pham, T.A., Wanunu, M., Noy, A., and Noy, A. (2017). Enhanced water permeability and tunable ion selectivity in subnanometer carbon nanotube porins. Science *359*, 792–796. https://doi.org/10.1126/science.aan2438.

92. Dellago, C., Naor, M.M., and Hummer, G. (2003). Proton transport through water-filled carbon nanotubes. Phys. Rev. Lett. *90*, 105902. https://doi.org/10.1103/PhysRevLett.90.105902.

93. Cao, Z., Peng, Y., Yan, T., Li, S., Li, A., and Voth, G.A. (2010). Mechanism of fast proton transport along one-dimensional water chains confined in carbon nanotubes. J. Am. Chem. Soc. *132*, 11395–11397. https://doi.org/10.1021/ja1046704.

94. Andrei, I.M., and Barboiu, M. (2022). Biomimetic artificial proton channels. Biomolecules *12*, 1473–1525. https://doi.org/10.3390/biom12101473.

95. Zhang, H., Li, X., Hou, J., Jiang, L., and Wang, H. (2022). Angstrom-scale ion channels towards single-ion selectivity. Chem. Soc. Rev. *51*, 2224–2254. https://doi.org/10.1039/d1cs00582k.

96. Si, W., Xin, P., Li, Z.T., and Hou, J.L. (2015). Tubular unimolecular transmembrane channels: construction strategy and transport activities. Acc. Chem. Res. *48*, 1612–1619. https://doi.org/10.1021/acs.accounts.5b00143.

97. Eisenberg, B. (2003). Why can't protons move through water channels? Biophys. J. *85*, 3427–3428. https://doi.org/10.1016/S0006-3495(03)74763-8.

98. Strilets, D., Fa, S., Hardiagon, A., Baaden, M., Ogoshi, T., and Barboiu, M. (2020). Biomimetic approach for highly selective artificial water channels based on tubular pillar[5]arene dimers. Angew. Chem., Int. Ed. Engl. *132*, 23413–23419. https://doi.org/10.1002/ANGE.202009219.

99. Yan, Z.J., Wang, D., Ye, Z., Fan, T., Wu, G., Deng, L., Yang, L., Li, B., Liu, J., Ma, T., et al. (2020). Artificial aquaporin that restores wound healing of impaired cells. J. Am. Chem. Soc. *142*, 15638–15643. https://doi.org/10.1021/jacs.0c00601.

100. Yang, W., and de Villiers, M.M. (2005). Effect of 4-sulphonato-calix[n]arenes and cyclodextrins on the solubilization of niclosamide, a poorly water soluble anthelmintic. AAPS J. *7*, E241–E248. https://doi.org/10.1208/aapsj070123.

101. Eddaif, L., Shaban, A., and Telegdi, J. (2019). Sensitive detection of heavy metals ions based on the calixarene derivatives-modified piezoelectric resonators: a review. Int. J. Environ. Anal. Chem. *99*, 824–853. https://doi.org/10.1080/03067319.2019.1616708.

102. Ming, E., Tsang, W., Shi, Z., and Holdcroft, S. (2011). Ionic Purity and Connectivity of Proton-Conducting Channels in Fluorous-Ionic Diblock Copolymers, pp. 8845–8857.

103. Golubenko, D.V., Van der Bruggen, B., and Yaroslavtsev, A.B. (2021). Ion exchange membranes based on radiation-induced grafted functionalized polystyrene for high-performance reverse electrodialysis. J. Power Sources *511*, 230460–230511. https://doi.org/10.1016/j.jpowsour.2021.230460.

104. Chang, Y., Brunello, G.F., Fuller, J., Hawley, M., Kim, Y.S., Disabb-Miller, M., Hickner, M.A., Jang, S.S., and Bae, C. (2011). Aromatic ionomers with highly acidic sulfonate groups: acidity, hydration, and proton conductivity. Macromolecules *44*, 8458–8469. https://doi.org/10.1021/ma201759z.

105. Ahmad, S., Nawaz, T., Ali, A., Orhan, M.F., Samreen, A., and Kannan, A.M. (2022). An overview of proton exchange membranes for fuel cells: materials and manufacturing. Int. J. Hydrogen Energy *47*, 19086–19131. https://doi.org/10.1016/j.ijhydene.2022.04.099.

106. Cousins, I.T., Goldenman, G., Herzke, D., Lohmann, R., Miller, M., Ng, C.A., Patton, S., Scheringer, M., Trier, X., Vierke, L., et al. (2019). The concept of essential use for determining when uses of PFASs can be phased out. Environ. Sci. Process. Impacts *21*, 1803–1815. https://doi.org/10.1039/c9em00163h.

107. Di Vona, M.L., Sgreccia, E., Tamilvanan, M., Khadhraoui, M., Chassigneux, C., and Knauth, P. (2010). High ionic exchange capacity polyphenylsulfone (SPPSU) and polyethersulfone (SPES) cross-linked by annealing treatment: thermal stability, hydration level and mechanical properties. J. Membr. Sci. *354*, 134–141. https://doi.org/10.1016/j.memsci.2010.02.058.

108. Furer, V.L., Vandyukov, A.E., Khamatgalimov, A.R., Kleshnina, S.R., Solovieva, S.E., Antipin, I.S., and Kovalenko, V.I. (2019). Investigation of hydrogen bonding in p-sulfonatocalix [4] arene and its thermal stability by vibrational spectroscopy. J. Mol. Struct. *1195*, 403–410. https://doi.org/10.1016/j.molstruc.2019.06.008.

109. DSC Measurements of Polystyrene-The Effects of Molecular Weight on Glass Transition (1995). https://www.hitachi-hightech.com/file/global/pdf/products/science/appli/ana/thermal/application_TA_068e.pdf.

110. Rieger, J. (1996). The glass transition temperature of polystyrene. Results of a round robin test. J. Therm. Anal. *46*, 965–972. https://doi.org/10.1007/BF01983614.

111. Kushner, D.I., Zhu, L., Kusoglu, A., and Hickner, M.A. (2016). Side chain influence on the mechanical properties and water uptake of confined comb-shaped cationic polymer thin films. Macromol. Chem. Phys. *217*, 2442–2451. https://doi.org/10.1002/macp.201600254.

112. Zawodzinski, T.A., Springer, T.E., Davey, J., Jestel, R., Lopez, C., Valerio, J., and Gottesfeld, S. (1993). A comparative study of water uptake by and transport through ionomeric fuel cell membranes. J. Electrochem. Soc. *140*, 1981–1985. https://doi.org/10.1149/1.2220749.

113. Holz, M., Heil, S.R., and Sacco, A. (2000). Temperature-dependent self-diffusion coefficients of water and six selected molecular liquids for calibration in accurate 1H NMR PFG measurements. Phys. Chem. Chem. Phys. *2*, 4740–4742. https://doi.org/10.1039/b005319h.

114. English, N.J., and MacElroy, J.M.D. (2003). Hydrogen bonding and molecular mobility in liquid water in external electromagnetic fields. J. Chem. Phys. *119*, 11806–11813. https://doi.org/10.1063/1.1624363.

115. Horner, A., Zocher, F., Preiner, J., Ollinger, N., Siligan, C., Akimov, S.A., and Pohl, P. (2015). The mobility of single-file water molecules is governed by the number of H-bonds they may form with channel-lining residues. Sci. Adv. *1*, e1400083–e1400086. https://doi.org/10.1126/sciadv.1400083.

116. Song, W., Joshi, H., Chowdhury, R., Najem, J.S., Shen, Y.X., Lang, C., Henderson, C.B., Tu, Y.M., Farell, M., Pitz, M.E., et al. (2020). Artificial water channels enable fast and selective water permeation through water-wire networks. Nat. Nanotechnol. *15*, 73–79. https://doi.org/10.1038/s41565-019-0586-8.

117. Ye, G., Janzen, N., and Goward, G.R. (2006). Solid-state NMR study of two classic proton conducting polymers: nafion and sulfonated poly (ether ether ketone)s. Macromolecules *39*, 3283–3290. https://doi.org/10.1021/ma0523825.

118. Murata, K., Mitsuoka, K., Hirai, T., Walz, T., Agre, P., Heymann, J.B., Engel, A., and Fujiyoshi, Y. (2000). Structural determinants of water permeation through aquaporin-1.

Nature *407*, 599–605. https://doi.org/10.1038/35036519.

119. Reimer, U., Ehlert, J., Janßen, H., and Lehnert, W. (2016). Water distribution in high temperature polymer electrolyte fuel cells. Int. J. Hydrogen Energy *41*, 1837–1845. https://doi.org/10.1016/j.ijhydene.2015.11.106.

120. Nandi, P.K., and English, N.J. (2016). Role of hydration layer in dynamical transition in proteins: insights from translational self-diffusivity. J. Phys. Chem. B *120*, 12031–12039. https://doi.org/10.1021/acs.jpcb.6b06683.

121. Kobayashi, A., Fujii, T., Harada, C., Yasumoto, E., Takeda, K., Kakinuma, K., and Uchida, M. (2021). Effect of Pt and ionomer distribution on polymer electrolyte fuel cell performance and durability. ACS Appl. Energy Mater. *4*, 2307–2317. https://doi.org/10.1021/acsaem.0c02841.

122. Sambandam, S., and Ramani, V. (2010). Influence of binder properties on kinetic and transport processes in polymer electrolyte fuel cell electrodes. Phys. Chem. Chem. Phys. *12*, 6140–6149. https://doi.org/10.1039/b921916a.

123. Maurya, S., Dumont, J.H., Villarrubia, C.N., Matanovic, I., Li, D., Kim, Y.S., Noh, S., Han, J., Bae, C., Miller, H.A., et al. (2018). Surface adsorption affects the performance of alkaline anion-exchange membrane fuel cells. ACS Catal. *8*, 9429–9439. https://doi.org/10.1021/acscatal.8b03227.

124. Wang, J., Shi, Z., Zang, Y., Jia, H., Teraguchi, M., Kaneko, T., and Aoki, T. (2021). Macromolecular design for oxygen/nitrogen permselective membranes-top-performing polymers in 2020-. Polymers *13*, 3012–3039. https://doi.org/10.3390/polym13173012.